NANO LETTERS

2005
Vol. 5, No. 7
1509−1514

Biocompatible Force Sensor with Optical Readout and Dimensions of 6 nm^3

Hari Shroff,[†,§] Björn M. Reinhard,[‡,§] Merek Siu,[†,§] Harish Agarwal,[‡] Andrew Spakowitz,[‡] and Jan Liphardt*[,†,‡,§]

Biophysics Graduate Group and Department of Physics, University of California, Berkeley, California 94720, and Physical Biosciences Division, Lawrence Berkeley National Lab, Berkeley, California 94720

Received May 10, 2005; Revised Manuscript Received June 6, 2005

ABSTRACT

We have developed a nanoscopic force sensor with optical readout. The sensor consists of a single-stranded DNA oligomer flanked by two dyes. The DNA acts as a nonlinear spring: when the spring is stretched, the distance between the two dyes increases, resulting in reduced Förster resonance energy transfer. The sensor was calibrated between 0 and 20 pN using a combined magnetic tweezers/single-molecule fluorescence microscope. We show that it is possible to tune the sensor's force response by varying the interdye spacing and that the FRET efficiency of the sensors decreases with increasing force. We demonstrate the usefulness of these sensors by using them to measure the forces *internal* to a single polymer molecule, a small DNA loop. Partial conversion of the single-stranded DNA loop to a double-stranded form results in the accumulation of strain: a force of approximately 6 pN was measured in the loop upon hybridization. The sensors should allow measurement of forces internal to various materials, including programmable DNA self-assemblies, polymer meshes, and DNA-based machines.

Mechanical forces in the picoNewton (pN) range are generated in numerous chemical and biological processes. Several groups have reported DNA-based actuators,[1] tweezers,[2] or motors,[3] in which controlled conversion of single- to double-stranded DNA is exploited to build up strain, which is released by a subsequent displacement. Mechanical forces are also generated by biological machines, including during DNA transcription,[4,5] replication,[6] packaging of viral genomes,[7] and the movement of cargo inside the cell by myosin[8] and kinesin.[9]

With the maturation of technologies such as high-resolution tracking of single fluorophores,[10] it is now possible to watch individual molecular machines undergo conformational changes as they carry out their functions. However, a full understanding of small machines and devices, and the ability to construct them, requires knowledge not only of the displacements but also the forces involved. Once both the displacement and forces have been measured, the energetics of the reaction cycle are obtained immediately by integrating the force along the displacement. The measurement of mechanical force is thus desirable both from the perspective of designing the next generation of nanoscale machines and in order to understand the function of existing biological machines.

Mechanical measurements on single molecules and enzymes are typically undertaken in vitro using tools such as atomic force microscopy,[12,11] optical[13] and magnetic tweezers,[14] and microneedles.[15] Although these technologies provide an excellent means to exert pN forces on single molecules, they suffer from several technical limitations. First, in typical force studies, a system of interest (with a characteristic length scale of several nm) is mechanically coupled to a micron-sized polystyrene or magnetic bead, which dampens the system's dynamics. Second, conventional force-measuring technologies are limited in practice to a single spatial axis, defined by the vector connecting the attachment points of the measurement apparatus to the sample. Finally, it would be highly desirable to be able to characterize individual devices or machines near surfaces and membranes and in complex environments such as inside living cells with minimal external perturbations.[16]

Here we present a nanoscale force sensor capable of overcoming the problems outlined above and that can be inserted directly into molecular machines and small systems. The sensor consists of an entropic spring, single-stranded DNA (ssDNA), to which two fluorescent dyes are covalently attached. When force is exerted along the length of the molecule, the distance between the two dye molecules increases, resulting in reduced FRET (Förster resonance energy transfer) efficiency between the two dyes. The optical

* Corresponding author. Phone: 1-510-642-3578. E-mail: liphardt@physics.berkeley.edu.
† Biophysics Graduate Group, University of California, Berkeley.
‡ Department of Physics, University of California, Berkeley.
§ Physical Biosciences Division, Lawrence Berkeley National Lab.

10.1021/nl050875h CCC: $30.25
Published on Web 06/18/2005

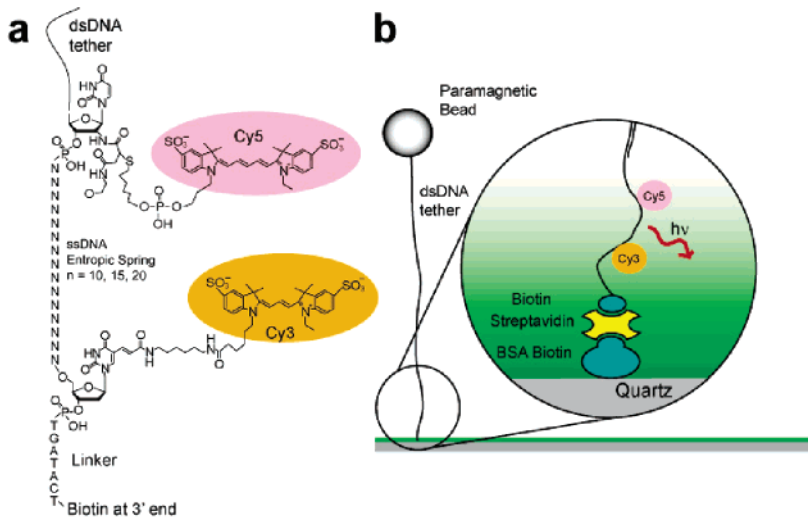

Figure 1. Diagram of force sensors and experimental geometry. (a) Force sensors were composed of Cy3/Cy5 dyes separated with single-stranded DNA of variable length. Details of linker attachment between dyes and backbone are shown. N denotes nucleotide. (b) Force sensor complexes were assembled in flow chambers and stretched with magnetic tweezers. Inset: Chambers were treated successively with Biotin-BSA and streptavidin. Double-stranded DNA formed a molecular handle between the magnetic bead and the top end of the sensor. On the bottom end, biotin provided an attachment point to the streptavidin-coated chamber. Sensors were excited with an evanescent wave (green gradient).

readout of the FRET efficiency thus constitutes a noninvasive measurement of the mechanical force acting on the sensor.

Several physical principles could be utilized to design a nanoscale force sensor, including mechanical deformation of covalent bonds in a dye molecule or compressing a quantum dot, which would change the system's energy levels in a force-dependent manner. However, such deformations require relatively high forces (>100 pN) and we wished to cover forces typical of many biological and nanotechnological force-generation processes, 0−20 pN.[17]

Rather than basing our sensors on direct energy-level modulation, we built a FRET-based sensor composed of an entropic spring and two dye molecules. Substantial straightening of a single entropic spring such as a nucleic acid or a polysaccharide from an isotropic random coil configuration typically requires forces much below 100 pN. In determining a suitable polymer for the entropic spring element, we considered both the desired force measurement range and the optimal spacing between the dye molecules. For a typical dye pair such as Cy3/Cy5 (Förster distance approximately 6 nm[18]), FRET is most useful in measuring length changes in the 4−7 nm range.

These two design criteria exclude many biological polymers. For example, double-stranded DNA (dsDNA) has a persistence length of approximately 50 nm.[19] At length scales below 10 nm, dsDNA behaves like a stiff rod; there is a negligible change in length over the desired force range. Therefore, we needed a less rigid polymer. We decided to use ssDNA as the entropic spring because it is well characterized[18,19] at the single-molecule level and is straightforward to synthesize, functionalize, and couple to biomolecules. The persistence length of ssDNA has been estimated to be 1−4 nm,[18,19] on order of the Cy3/Cy5 Förster distance. A 15-base piece of ssDNA has a contour length of approximately 9.5 nm, the upper end of distances accessible by FRET. This length is realizable experimentally by stretching the DNA to high forces. However, at zero force, the end-to-end distance would on average be less than 9.5 nm because of the intrinsic entropic elasticity of the polymer. These considerations suggest that a spring element with fluorescent dyes spaced approximately 15 bases apart might show significant changes in the FRET efficiency as force is applied. We investigated the force dependence of FRET for sensors with 10 (FS10), 15 (FS15), and 20 (FS20) bases spaced between Cy3 and Cy5 dyes (Figure 1a).

Bulk fluorescence assays were performed to verify the presence of both dyes on the force sensors. As expected, the FRET efficiencies decrease with increasing spacer length (Figure 3a). To investigate the dependence of the FRET efficiency on force, we next characterized the fluorescence properties of the sensors at the single-molecule level.

We began our characterization of single force sensors by determining their fluorescence properties at zero force. The force sensor constructs were immobilized on the surface of a homemade flow cell with a biotin−streptavidin system and excited using total internal reflection fluorescence microscopy (Figure 1b). We determined the magnitude of the FRET efficiency, E, for sensors FS10, FS15, and FS20. As shown in Figure 3b, the FRET efficiency decreased with increasing spacer length, as expected. Next, we determined the effect of attaching long dsDNA handles (λ DNA, 16.4 μm) to the force sensors. We were concerned that at low forces the local dielectric constant would be modified by the handles, with consequent changes in the fluorescence properties of the dyes and thus the magnitude of energy transfer. We were also worried that attaching a long polymer to the sensor would modify the mechanical properties of the sensors. However, as seen in Figure 3c, the FRET efficiency of the sensors with λ DNA (+ handles) was statistically indistinguishable from the previous experiments with sensors lacking λ DNA

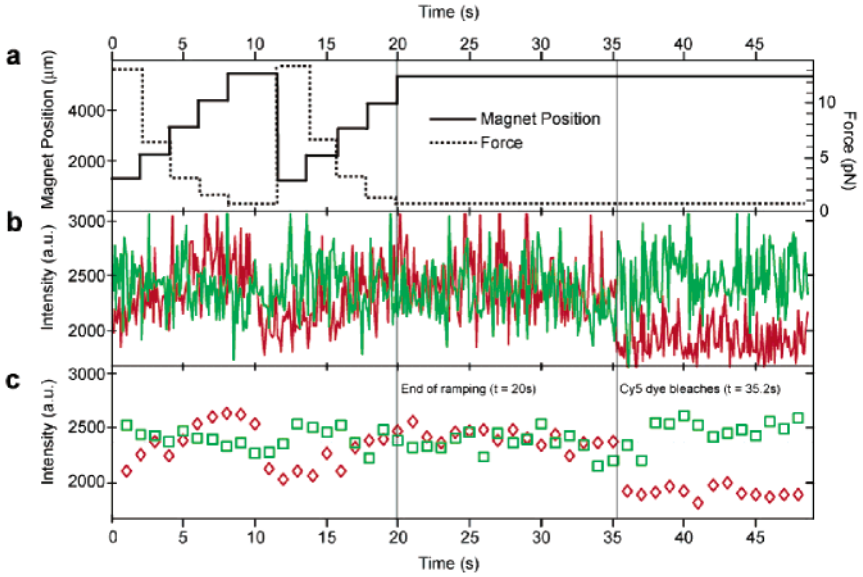

Figure 2. A typical ramping experiment. (a) Magnet positions and corresponding forces. (b) Single-molecule FRET trace for force sensor with 20 base spacing between Cy3 (green) and Cy5 (red). (**c**) Trace in (b) is averaged in 1-s intervals. Ramping is completed after 20 s, and the Cy5 dye bleaches after 35.2 s.

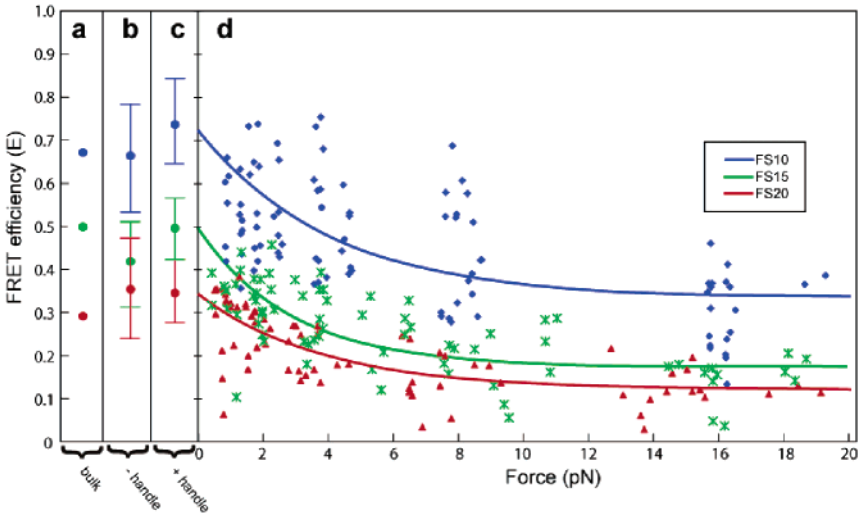

Figure 3. FRET efficiency (E) values. (a) The bulk values of FRET efficiency were determined to be 0.67, 0.50, and 0.29, for FS10, FS15, and FS20, respectively. (b) The FRET efficiencies for the unligated sensors (− handles) at zero force were determined to be (mean ± standard deviation) 0.66 ± 0.13, $N = 14$; 0.41 ± 0.10, $N = 11$; 0.35 ± 0.11, $N = 6$ for FS10, FS15, and FS20, respectively. Total number of data points, FS10−20: 213, 107, 91. (c) The FRET efficiencies for the ligated sensors (+ handles) at zero force were determined to be 0.74 ± 0.10, $N = 9$; 0.50 ± 0.08, $N = 7$; 0.34 ± 0.08, $N = 8$, for FS10, FS15, and FS20, respectively. Total number of data points, FS10−20: 103, 119, 81. (d) Force versus FRET efficiency. The total number, N, of force sensor complexes (force sensor + λ DNA handles + magnetic beads) analyzed for each dye spacing was 11, 8, and 11, for FS10, FS15, and FS20, respectively. Data and three parameter exponential fits are shown (FS10, $E(f) = 0.34 + 0.39 \exp(-0.25f)$, $r^2 = 0.65$; FS15, $E(f) = 0.17 + 0.32 \exp(-0.35f)$, $r^2 = 0.71$; FS20, $E(f) = 0.12 + 0.22 \exp(-0.26f)$, $r^2 = 0.60$). The large number of data points for zero force (whose means and standard deviations are shown in panel c) are not shown for clarity.

(− handles). Furthermore, the single-molecule FRET efficiencies at zero force agree well with the bulk efficiencies.

Having established the properties of the force sensors at zero force, we determined their response to external forces. Force sensors with λ DNA handles were attached to paramagnetic beads (Figure 1b), and magnetic tweezers were used to exert pN range forces on the complexes. To find suitable bead/force sensor complexes, the microscope was focused on the bottom surface of the chamber using total internal reflection excitation; force sensors appeared as bright spots against a dark background. The sample chamber was then examined using brightfield illumination. Tethered beads appeared as out-of-focus circles in the field of view. Once a suitable tether had been found, the brightfield excitation was turned off, the sensor was excited, and the external force was ramped between 1 and 20 pN by changing the position of the magnets.

The position of the magnets and force versus time for a typical ramping experiment are shown in Figure 2a. The corresponding fluorescence intensity versus time trace for a

single force sensor (raw data for a dye separation of 20 bases) is shown in Figure 2b. The Cy3 (donor) channel is shown in green, and the Cy5 (acceptor) channel is shown in red. Figure 2c shows the same trace averaged; each point represents the average of 10 frames (1 s) of data from Figure 2b. As the magnet position is raised to decrease the force on the sensor, the Cy5 fluorescence increases and the Cy3 fluorescence decreases. We expect this behavior because at low forces, the two dyes will on average be closer together than at high forces and thus there will be more FRET. At 20 s, after the second magnet ramp, the position of the magnets is kept fixed until the end of the experiment. The corresponding fluorescence intensity on each channel stays relatively constant until 35.2 s, when the Cy5 dye bleaches.

Data were taken for multiple complexes along the length of the chamber. A typical chamber yielded fluorescence intensity versus force traces for 1−3 tethered beads. We show the FRET efficiency versus force for each kind of sensor in Figure 3d. In general, the data are sparser at the higher force values because of the exponential relation between magnet position and force. At zero force, the FRET efficiency of the sensor with 10 bases between the dyes is greater than the sensor with 20 bases (Figure 3c) with the 15-base sensor falling between the two values. This trend persists throughout the range of forces we measured, so the data are consistent with our expectation that a larger spacing between the dyes leads to reduced FRET efficiency.

In these single-molecule experiments, a known force was applied and the resulting FRET efficiency was determined (Figure 3). However, experimentalists wishing to determine the force from a series of FRET measurements will face the opposite situation. How can one extract estimates of the force from FRET measurements, and how good will these estimates be? We estimated the force resolution of our sensors by inverting the exponential fits to obtain force as a function of FRET efficiency and then propagating the measured standard deviations in the efficiency. The mean and standard deviation of the FRET efficiency for the FS10 sensor at 2 ± 1 pN is 0.5 ± 0.1. The corresponding forces are 1.1−5.7 pN. A similar range is found for the FS15 and FS20 data.

These values suggest a resolution of approximately 5 pN for the high-FRET range. This resolution is comparable to AFM but lower than that achievable by optical tweezers. Reducing sources of instrumental noise (e.g., intensifier noise, read noise, and dark noise) will result in a reduced spread and thus a better resolution. We note that the resolution of our sensors is dependent on force: because the efficiencies plateau as a function of increasing force, the resolution decreases with increasing force.

We found that all three sensors were able to distinguish between high (15−20 pN) and low (0−5 pN) forces (Figure 4). For a given value of E, how certain are we that it belongs in either distribution? An experimentally useful quantity is a "cutoff" value of the efficiency, E_c, where all values of E less than E_c are assigned to the high force distribution, and all values of E greater than E_c are assigned to the low force distribution. For our sensors, the values of E_c that reduce the number of incorrect assignments to below 10% are shown in the Figure 4 legend.

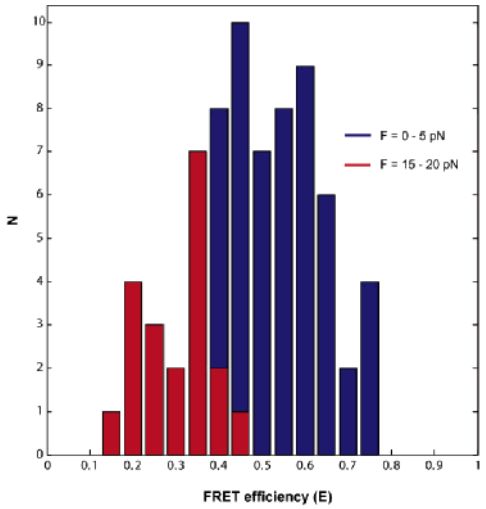

Figure 4. Distributions of E values for high (15−20 pN, red) and low (0−5 pN, blue) forces for FS10 data. Bars that are both blue and red indicate overlap of distributions. Bins are spaced every 0.05 efficiency units. E_c for FS10: 0.38, 92% correct assignments; E_c for FS15: 0.22, 96% correct assignments; E_c for FS20: 0.14, 92% correct assignments.

A primary use of our sensors is measuring forces in situations where conventional single-molecule manipulation tools fail. For example, several groups have reported self assemblies of DNA tiles[20,21] or bundles,[22] where it is difficult to imagine how one would measure the distribution of forces internal to these materials. To illustrate the applicability and usefulness of our sensors for this type of application, in which pN range forces are to be measured in situ, we used them to determine the forces inside a 37 nucleotide DNA loop.

We constructed single-stranded DNA loops using CircLigase, a thermostable ATP-dependent ligase that efficiently circularizes linear ssDNA. We designed a 37-mer, FS10-L, with Cy3 and Cy5 dyes, and the same sequence between the two dyes as FS10. FS10 was chosen as the force-sensing element because it displayed the greatest change in FRET efficiency as a function of force.

The bulk FRET efficiency of FS10-L was $E = 0.70$, practically indistinguishable from the FRET efficiency of FS10, $E = 0.67$. The similarity in FRET values suggests that the base changes in the regions flanking the sensor sequence have a negligible effect on its properties.

Next, the FS10-L oligo was incubated with CircLigase, and the slower migrating reaction product was gel purified. To confirm that DNA circles had indeed been formed, we incubated the unligated FS10-L and the ligated FS10-L samples with Exonuclease I, which degrades linear ssDNA. The unligated force sensor was degraded readily, but the ligated FS10-L was resistant toward the exonuclease, suggesting that it was circular. The FRET efficiency of the FS10-L circles was 0.78 and thus somewhat increased compared to the unligated FS10-L (Figure 5). This result is expected based on the properties of a Gaussian chain because circularization will bring any two points on the polymer closer (see below). Finally, we added a 25 base DNA

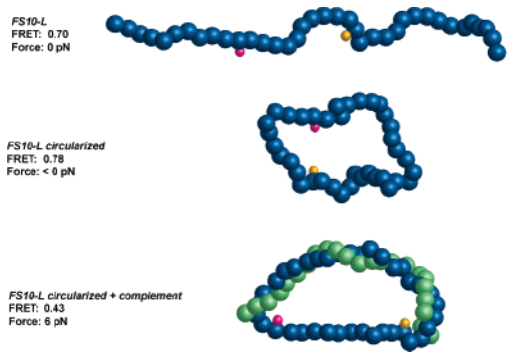

Figure 5. Schematic depiction of loop constructs with measured bulk FRET values and force sensor readouts. Forces are positive when pulling the two dyes apart. Blue and green chains represent DNA oligos, orange and pink circles represent Cy3 and Cy5 dyes.

oligonucleotide that was complementary to the part of the circle directly opposite the sensor. Upon annealing, the FRET efficiency dropped to 0.43, implying that the circles were now more strained than before (Figure 5).

Are the measured FRET changes consistent with theory? For simplicity, we modeled the single-stranded DNA segments within our constructs as Gaussian chains.[23] Undoubtedly, more sophisticated models for RNA and single-stranded DNA exist that incorporate the interplay among electrostatics, base-pairing, and base-pair stacking.[24,25,26] However, the Gaussian chain model captures the general features inherent in our experiments and has the advantage of being analytically tractable. The double-stranded DNA segments are modeled as linear elastic filaments,[27] which is the athermal limit to the wormlike chain model[28] that is appropriate for the short lengths in our experiments. Again, more sophisticated models exist for short lengths of double-stranded DNA that incorporate such effects as stress-induced melting.[29] Defining the Förster distance as R_0, the FRET efficiency is given by

$$E = \int \mathrm{d}\vec{R}\, \frac{R_0^6}{R^6 + R_0^6}\, G(\vec{R})$$

where $G(\vec{R})$ is replaced by the appropriate distribution function for a linear chain or a ring (please see the Supporting Information for these functions).

The first construct in our experiments is ssDNA of total length 37 bases with FRET dyes separated by 10 bases. Setting the Förster distance, R_0, to 6 nm, the length per base, l, as 0.71 nm, and the Kuhn length, $b = 2l_p$, to 4 nm (comparable to previous measurements of ssDNA rigidity[24,25,26]), we predict the FRET efficiency of this linear construct to be 0.69, which was experimentally determined to be 0.70.

The second construct in our experiments is a ssDNA ring of total length 37 bases with 10 bases separating the FRET dyes. With the same parameters as above, we calculate the FRET efficiency to be 0.79, as compared to the experimental measurement of 0.78. Because our calibration experiments did not investigate the response of the sensor to negative tension, we cannot extract a force for the single-stranded loop.

In the last set of experiments, we added complementary DNA to the single-stranded ring (Figure 5), yielding, upon hybridization, a DNA ring with a single-stranded force-sensor section with 10 bases and a double-stranded section with 25 base-pairs. By comparison with our force-sensor calibration data, we find the FRET efficiency of 0.43 of this construct corresponds to approximately 6 pN of tension of the strand.

Because the rigidity of the double-stranded section is substantially larger than its single-stranded analogue, the 10-base single-strand section is stretched upon hybridization of the 25-base section. However, the single-strand section is not fully extended to its contour length, which would result in a FRET efficiency of 0.27 (predicted by a Förster length, R_0, of 6 nm and dye separation of 7.1 nm). The analysis performed for the distance between dye segments for the linear and looped constructs cannot be used for partially double-stranded loops because the Gaussian chain model does not accommodate the fixed contour length that is required to capture the behavior for this amount of extension.

Instead, we compare the experimentally determined tension applied on the force sensor with the force required to bend a short double-stranded DNA strand into a loop according to the wormlike chain model. Modeling the double-stranded section as a linear elastic rod, the onset of looping occurs when the dimensionless group $fL^2/(k_BTl_p)$ exceeds a value of π^2,[27] where f is the tension, L is the contour length (9.18 nm), k_BT is the thermal energy (4.1 pN nm), and l_p is the persistence length of double-stranded DNA (53 nm). This corresponds to a tension of 25.4 pN, revealing that the measured force is lower than the theoretical prediction.

Assuming an error of ± 5 pN on the experimentally measured force of 6 pN, the upper bound of 11 pN is still less than the 25.4 pN value predicted from the wormlike chain model of polymer elasticity. This discrepancy suggests a bend softening of the tightly bent double-stranded section in our experiments, which could be explained by a number of physical mechanisms including strain-induced melting, major-minor groove bending discrepancies, and substantial fraying of the DNA at the junction between single- and double-stranded sections.

In addition to characterization of DNA loops, the experiments presented here suggest several applications for the force sensors. Several DNA-based nanodevices[1,2,3] already contain ssDNA. The addition of a FRET pair would readily allow measurement of the forces experienced (or generated) by these devices. Furthermore, although fabrication of one- or two-dimensional DNA assemblies has been reported,[20,21,22] there is a lack of direct measurement of strains and stresses in these structures because previous experimental tools are not amenable to this kind of measurement. Insertion of force sensors directly into DNA tiles would reveal their response to external forces. Tiles with internal strain gauges would also assist in the design of 3D lattices based on controlled

introduction of strains into the material or facilitate efforts to make 2D assembly more robust, based on minimizing such strains.

For use outside of materials science and nanotechnology, such as in cell biology, several properties of the sensors should be refined. The useful lifetime of our FRET sensors was limited by the lifetime of the Cy5 dye to about 20 s, even though an oxygen scavenger system was employed. Inside a living cell, the expected lifetime will be even shorter because oxygen levels will be higher than those in our flow chamber. Replacing the dye molecules with noble metal nanoparticles should increase the sensor's lifetime indefinitely; in this case the observable would be a shift in interparticle plasmon resonance[30,31] rather than FRET efficiency. Moreover, a biologically inert polymer, such as peptide nucleic acid,[32] should be used as the spring to alleviate undesired sensor−protein interactions.

Using different materials for the spring also allows one to tune the sensor to various force ranges. As for any other strain gauge, there will be a tradeoff between force resolution and dynamic range, with smaller persistence lengths leading to increased dynamic range but lower force resolution. The sensor's force range can also be tuned by adjusting the spring length (Figure 3) and/or sequence, based on the known dependence of the ssDNA's mechanical properties on base stacking and other sequence effects.[24]

Attachment of the sensor to appropriate points on a biological molecular machine should allow force measurement along arbitrary axes. Attaching several sensors at once to different positions on the machine might allow simultaneous determination of the force along multiple spatial reaction coordinates. As demonstrated in the loop experiments, the sensors need not be attached to the machine itself but instead can be attached to its substrate.

Finally, as with any force sensor, microscopic or macroscopic, attachment geometry plays a role in determining its mechanical response. The behavior of two springs in parallel is different than their behavior in series. In our calibration experiments, the force acting on the sensor was identical to the force acting on the λ DNA because they were connected in series. However, the force is not distributed equally if the sensor is placed in parallel with another spring, such as a protein α helix. This effect can be minimized by choosing a polymer with a small spring constant.

Acknowledgment. We thank Thorsten Hugel, Jacob Siegel, Jeff Gore, and Arthur Edelstein for critically reading this manuscript, Nikolai Polouchine for helpful discussions, and Carlos Bustamante for generous use of equipment and facilities. H.S. holds a fellowship from the Fannie and John Hertz Foundation and B.R. acknowledges support from the Otto A. Wipprecht foundation and Deutsche Forschungsgemeinschaft. M.S. is supported by a Howard Hughes Predoctoral Fellowship and H.A. is supported by a National Science Foundation Graduate Research Fellowship. J.T.L. is supported by the Director's Fellowship of Lawrence Berkeley National Lab. This work was supported by Department of Energy grants DE-AC03-76SF00098 and W-7405-ENG-36.

Supporting Information Available: DNA sequences, methods, and description of hybrid instrument. This material is available free of charge via the Internet at http://pubs.acs.org.

References

(1) Simmel, F. C.; Yurke, B. *Phys. Rev. E* **2001**, *63*, 041913.
(2) Yurke, B.; Turberfield, A. J.; Mills, A. P., Jr.; Simmel, F. C.; Neumann, J. L. *Nature* **2000**, *406*, 605−608.
(3) Sherman, W. B.; Seeman, N. C. *Nano Lett.* **2004**, *4*, 1203−1207.
(4) Wang, M. D.; Schnitzer, M. J.; Yin, H.; Landick, R.; Gelles, J.; Block, S. M. *Science* **1998**, *282*, 902−907.
(5) Shaevitz, J. W.; Abbondanzieri, E. A.; Landick, R.; Block, S. M. *Nature* **2003**, *426*, 684−687.
(6) Wuite, G. J.; Smith, S. B.; Young, M.; Keller, D., Bustamante, C. *Nature* **2000**, *404*, 103−106.
(7) Smith, D. E.; Tans, S. J.; Smith, S. B.; Grimes, S.; Anderson, D. L.; Bustamante, C. *Nature* **2001**, *413*, 748−752.
(8) Mehta, A. D.; Rock, R. S.; Rief, M.; Spudich, J. A.; Mooseker, M. S.; Cheney, R. E. *Nature* **1999**, *400*, 590−593.
(9) Kuo, S. C.; Sheetz, M. P. *Science* **1993**, *260*, 232−234.
(10) Yildiz, A.; Forkey, J. N.; McKenney, S. A.; Ha, T.; Goldman, Y. E.; Selvin, P. R. *Science* **2003**, *300*, 2061−2065.
(11) Fisher, T. E.; Oberhauser, A. F.; Carrion-Vazquez, M.; Marszalek, P. E.; Fernandez, J. M. *Trends Biochem. Sci.* **1999**, *24*, 379−384.
(12) Rief, M.; Gautel, M.; Oesterhelt, F.; Fernandez, J. M.; Gaub, H. E. *Science* **1997**, *276*, 1109−1112.
(13) Ashkin, A.; Dziedzic, J. M. *Science* **1987**, *235*, 1517−1520.
(14) Smith, S. B.; Finzi, L.; Bustamante, C. *Science* **1992**, *258*, 1122−1126.
(15) Kishino, A.; Yanagida, T. *Nature* **1988**, *334*, 74−76.
(16) Gross, P. *Methods Enzymol.* **2003**, *361*, 162−174.
(17) Bustamante, C.; Chemla, Y. R.; Forde, N. R.; Izhaky, D. *Annu. Rev. Biochem.* **2004**, *73*, 705−748.
(18) Murphy, M. C.; Rasnick, I.; Cheng, W.; Lohman, T. M.; Ha, T. *Biophys. J.* **2004**, *86*, 2530−2537.
(19) Smith, S. B.; Cui, Y. J.; Bustamante, C. *Science* **1996**, *271*, 795−799.
(20) Park, S. H.; Barish, R.; Li, H.; Reif, J. H.; Finkelstein, G.; Yan, H.; LaBean, T. H. *Nano Lett.* **2005**, *5*, 693−696.
(21) Park, S. H.; Yin, P.; Liu, Y.; Reif, J. H.; LaBean, T. H.; Yan, H. *Nano Lett.* **2005**, *5*, 729−733.
(22) Mathieu, F.; Liao, S.; Kopatsch, J.; Wang, T.; Mao, C.; Seeman, N. C. *Nano Lett.* **2005**, *5*, 661−665.
(23) Doi, M.; Edwards, S. F. *The Theory of Polymer Dynamics*, 1st ed.; Clarendon: Oxford, U.K., 1986.
(24) Zhang, Y.; Zhou, H.; Ou-Yang, Z.-C. *Biophys. J.* **2001**, *81*, 1133−1143.
(25) Gerland, U.; Bundschuh, R.; Hwa, T. *Biophys. J.* **2001**, *81*, 1324−1332.
(26) Dessinges, M.-N.; Maier, B.; Zhang, Y.; Peliti, M.; Bensimon, D.; Croquette, V. *Phys. Rev. Lett.* **2002**, *89*, 248102.
(27) Landau, L. D.; Lifshitz, E. M. *Theory of Elasticity*; Pergamon Press: Elmsford, NY, 1986.
(28) Kratky, O.; Porod, G. *Recl. Trav. Chim. Pays-Bas* **1949**, *68*, 1106.
(29) Marko, J. F.; Yan, J. *Phys. Rev. Lett.* **2004**, *93*, 108108.
(30) Su, K.-H.; Wei, Q.-H.; Zhang, X.; Mock, J. J.; Smith, D. R.; Schultz, S. *Nano Lett.* **2003**, *3*, 1087−1090.
(31) Atay, T.; Song, J.-H.; Nurmikko, A. V. *Nano Lett.* **2004**, *4*, 1627−1631.
(32) Nielsen, P. E. *Methods Mol. Biol.* **2005**, *288*, 343−358.

NL050875H